J. At. Mol. Sci.
doi: 10.4208/jams.042611.051411a

Vol. **3**, No. 1, pp. 1-22
February 2012

Molecular structure, vibrational spectroscopic (FT-IR, FT-Raman),first order hyperpolarizability, NBO analysis, HOMO and LUMO analysis, thermodynamic properties of 3,5-dimethylbenzophenone by *ab inito* HF and density functional method

K. Chaitanya*, C. Santhamma, K. V. Prasad, and V. Veeraiah

Molecular Spectroscopy Laboratories, Department of Physics, Andhra University, Visakhapatnam, India

Received 26 Arpil 2011; Accepted (in revised version) 14 May 2011
Published Online 28 September 2011

Abstract. The FT-IR solid phase (4000–450 cm^{-1}) and FT-Raman spectra (3500–100 cm^{-1}) of 3,5-Dimethylbenzophenone (3,5-DMBP) was recorded at room temperature. Density functional theory calculations with B3LYP/ 6-31+G(d, p) basis sets was used to determine ground state molecular geometries (bond lengths and bond angles), harmonic vibrational frequencies, infrared intensities, Raman activities and bonding features of this compound. The assignments of the vibrational spectra have been carried out with the help of normal co-ordinate analysis (NCA) following the Scaled Quantum Mechanical Force Field methodology (SQMFF). The first order hyperpolarizability (β_0) of this novel molecular system and related properties (β, α_0 and $\Delta\alpha$) of DMBP are calculated using HF/6-31+G(d,p) method on the finite-field approach. Stability of the molecule have been analyzed using NBO analysis. The calculated first hyperpolarizability shows that the molecule is an attractive molecule for future applications in non-linear optics. The calculated HOMO and LUMO energies show that charge transfer occurs within the molecule. Mulliken population analysis on atomic charges is also calculated. On the basis of vibrational analyses, the thermodynamic properties of the title compounds at different temperatures have been calculated. Finally the calculations results were applied to simulate infrared and Raman spectra of the title compound which show good agreement with observed spectra.

PACS: 33.20.Fb, 31.15.-p

Key words: 3, 5-dimethylbenzophenone, FT-IR, FT-Raman, NCA, NBO analysis

*Corresponding author. *Email address:* cskcmail@gmail.com (K. Chaitanya)

1 Introduction

Benzophenone and its derivatives were of great interest because of their extensive application in varied areas, such as medicine [1–3] and photochemistry [4, 5]. These molecules possess non-centro symmetry and hence they are widely used in the synthesis of molecules having non-linear responses [6, 7]. The investigation on the structure and fundamental vibrations of benzophenone and its derivatives are still being carried out increasingly. The inclusion of an electron donating methyl group in aromatic ring leads to the variation of charge distribution in the molecule, and consequently affects the structural, electronic and vibrational parameters.

The vibrational spectra of benzophenone and its derivatives were measured and discussed by several authors [8–23]. While the standard molar gas-phase enthalpies of formation, at T = 298.15 K, of 2-, 3-, and 4-methylbenzophenone [24] and 2,3-, 2,4-, 2,5-, 2,6-, 3,4-, 3,5-, 2,2'-, 2,3'-, 2,4'-, 3,3'-, 3,4'- and 4,4'- dimethylbenzophenone [25] have been studied both by experimental and computational techniques, there comprehensive normal-mode analysis is unavailable. Crystal, molecular structure and vibrational spectra of α-4-methylbenzophenone by density functional theory calculations have been carried out by Sasiadek *et al.* [26]. Literature survey reveals that so far there is no complete vibrational spectral study for the title compound 3,5-DMBP.

In the present study we have investigated the optimized geometries, atomic charges and vibrational spectra for the 3,5-DMBP molecule in optimum energy conformation and analyze the influences of methyl group to the geometry and different normal modes of the benzophenone molecule. The vibrational frequencies of the title compound are assigned to their corresponding normal mode vibration using band intensities and potential energy distributions (PEDs). The redistribution of electron density (ED) in various bonding, antibonding orbitals and $E(2)$ energies had been calculated by natural bond orbital (NBO) analysis to give clear evidence of stabilization originating from the hyper conjugation of various intra-molecular interactions. The study of HOMO, LUMO analysis have been used to elucidate information regarding charge transfer within the molecule. Finally, the thermodynamic properties of the optimized structures were obtained theoretically from the harmonic vibrations.

2 Experimental

Fourier transform infrared spectra of the title compound is measured at the room temperature in the region 4000–400 cm^{-1} using a BRUKER IFS -66 V FTIR spectrometer at a resolution of ± 1 cm^{-1} equipped with a MCT detector, a KBr beam splitter and globar source. The FT-Raman spectrum of 3,5-DMBP is recorded on a BRUKER IFS -66 V model interferometer equipped with FRA-106 FT-Raman accessory in the 3500–100 cm^{-1} Stokes region using the 1064 nm line of a Nd: YAG laser for excitation operating at 200 mW power. The reported wave numbers are believed to be accurate within ± 1 cm^{-1}. The molecule 3, 5-dimethylbenzophenone was newly synthesized by Wang *et al.* [27].

3 Computational details

As the first step the optimized molecular structure, energy, and vibrational frequencies of the molecule have been calculated by using B3 [28] exchange functional combined with the LYP [29] correlation functional resulting in the B3LYP density functional method at 6-31+G(d, p) basis set. All the computations were performed using Gaussian 03W program [30] and Gauss-View molecular visualization program package on the personal computer [31]. Secondly, a comparison is made between the theoretically calculated frequencies and the experimentally measured frequencies. In this investigation we observed that the calculated frequencies were slightly greater than the fundamental frequencies. To improve the agreement between the predicted and observed frequencies, the computed harmonic frequencies are usually scaled for comparison. In this work the scaling of the force field was performed according to the SQMFF procedure [32], the Cartesian representation of the force constants were transferred to a nonredundant set of local symmetry coordinates, chosen in accordance to the recommendations of Pulay *et al.* [33]. The descriptions of the predicted frequencies during the scaling process were followed by the potential energy distribution (PED) matrix. The characterization of the normal modes using potential energy distribution (PED) was done with the MOLVIB -7.0 program written by Sundius [34, 35]. The NBO calculations [36] were performed using NBO 3.1 program as implemented in the Gaussian 03W [30] package at the DFT/B3LYP level in order to understand the intra-molecular delocalization or hyperconjugation.

3.1 The prediction of Raman intensities

The Raman activity (S_i) calculated by Gaussian 03 and adjusted during scaling procedure with MOLVIB were converted to relative Raman intensity (I_i) using the following relation from the basic theory of Raman scattering [37, 38]

$$I_i = \frac{f(\nu_0 - \nu_i)^4 S_i}{\nu_i \left(1 - \exp\left(\frac{-hc\nu_i}{KT}\right)\right)},$$

Here ν_0 is the exciting frequency (in cm^{-1} units); ν_i is the vibrational wave number of the normal mode; h, c, k are the universal constants and f is suitably chosen common normalization factor for all the intensities. For the plots of simulated IR and Raman spectra, pure Lorentzian band shapes were used with a bandwidth (FWHM) of 10 cm^{-1}. The theoretically simulated spectra are more regular than the experimental ones, because many vibrations presenting in condensed phase leads to strong perturbation of infrared intensities of many other modes.

The second-order polarizability or first hyperpolarizability β, dipole moment μ and polarizability α was calculated using HF/6-31+ G(d, p) basis set on the basis of the finite-field approach. The complete equations for calculating the magnitude of total static dipole moment μ, the mean polarizability α_0, the anisotropy of the polarizability $\Delta\alpha$ and the mean first hyperpolarizability β_0, using the x, y, z components from Gaussian 03W output is defined as

follows

$$\mu = {\mu_x}^2 + {\mu_y}^2 + {\mu_z}^2,$$
$$\alpha_0 = \frac{\alpha_{xx} + \alpha_{yy} + \alpha_{zz}}{3},$$
$$\Delta\alpha = 2^{\frac{1}{2}}\left[(\alpha_{xx} - \alpha_{yy})^2 + (\alpha_{yy} - \alpha_{xx})^2 + 6\alpha_{xx}^2\right]^{\frac{1}{2}},$$
$$\beta = \left({\beta_x}^2 + {\beta_y}^2 + {\beta_z}^2\right)^{\frac{1}{2}},$$
$$\beta_x = \beta_{xxx} + \beta_{xyy} + \beta_{xzz}, \qquad \beta_y = \beta_{yyy} + \beta_{xxy} + \beta_{yzz}, \qquad \beta_z = \beta_{zzz} + \beta_{xxz} + \beta_{yyz}.$$

Since the values of the polarizabilities (α) and hyperpolarizability (β) of Gaussian 03 output are reported in atomic units (a.u), the calculated values have been converted into electrostatic units (esu) (α: 1 a.u = 0.1482 $\times$ 10^{-12} esu, β: 1 a.u = 8.6393 $\times$ 10^{-33} esu). The total molecular dipole moment and mean first hyperpolarizability of 3,5-DMBP is 3.6186 Debye and 1.12525 $\times$ 10^{-30} esu respectively shown in Table 1. Total dipole moment of title molecule is approximately 10 times greater than those of urea. The above results show that 3,5-DMBP is the best material for NLO applications.

Table 1: Calculated all β components and β_{tot} value of 3,5-DMBP.

	HF/6-31+G(d,p)
β_{xxx}	-141.65
β_{xxy}	-45.190
β_{xyy}	18.917
β_{yyy}	-25.779
β_{xxz}	-78.970
β_{xyz}	19.373
β_{yyz}	15.466
β_{xzz}	-0.1137
β_{yzz}	75.151
β_{zzz}	9.0258
β_{total} (esu)	1.12525×10^{-30}

3.2 Potential energy distribution

In the normal coordinate analysis by Wilson's GF matrix method [39]. It is possible to obtain useful information about the fundamental vibrational modes from the L matrix whose columns are the characteristic vectors of the GF matrix. The L matrix is given by the internal symmetry coordinate matrix R and the normal coordinate matrix Q as

$$R = LQ.$$

The potential energy V for the normal vibration associated with normal coordinate Q_k can be written in the form

$$V = \frac{1}{2}\sum_{i,j} F_{ij} R_i R_j = \frac{1}{2}\sum_k Q_k^2 \sum_{i,j} F_{ij} L_{jk} L_{ik},$$

where R_i is the internal coordinates and F_{ij} are the force constants. The quantities L_{ik} are the elements of the matrix of the vibrational modes L (the transformation matrix).

If the force constant matrix is known, one can compute $L_{jk}L_{ik}F_{ij}$ terms, and obtained a two-dimensional, symmetric matrix of these terms for each normal coordinate [40, 41]. Instead of these matrices, however, usually a single potential energy distribution matrix, PED, is applied, whose elements are given by

$$\left[PED\right]_{kj} = \sum_i L_{jk} L_{ik} F_{ij}.$$

Some authors prefer normalizing the matrix elements with respect to the calculated eigenvalues, λ_k, to obtain

$$\left[PED\right]^{\lambda}_{kj} = \frac{\sum_i L_{jk} L_{ik} F_{ij}}{\lambda_k}.$$

The distribution of potential energy in each internal coordinate is of great help in assigning the calculated vibrations of molecules. In many cases this distribution permits frequencies to be assigned to specific vibrations more reliably than the modes of vibration themselves.

4 Results and discussion

4.1 Molecular geometry

The structure of the molecule with numbering scheme for the atoms is presented in Fig. 1. The optimized structure parameters of 3,5-DMBP calculated by DFT /B3LYP level with 6-31 + G (d, p) basis sets are presented in Table 2. The results are compared with the available experimental data of similar systems, as data of crystal structure of 3,5-dimethylbenzophenone is not available [26, 42, 43]. The calculated C–C bond lengths of the ring vary from 1.37 to 1.40 Å. However, the phenyl ring appears to be a little distorted from its regular hexagonal symmetry as the computed bond lengths: C1–C2, C3–C4, and C5–C6 are larger and C2–C3, C4–C5, C6–C1 are shorter. Breakdown of the regular hexagonal symmetry of the phenyl ring is also evident from the decrease in values of the bond angles C2–C3–C4, C4–C5–C6 and the increase in values of the bond angles C1–C2–C3, C3–C4–C5. The changes in the bond length or frequency and breakdown of regular hexagonal symmetry of the phenyl ring are attributed to the changes in charge distribution on the carbon atoms of the phenyl ring on substitution with methyl group [43]. The structure of the molecule deviates significantly from planarity because the two phenyl rings are rotated around the C–C(O)–C axes: the phenyl rings are twisted relative to the planar group C–C(O)–C to give a C25–C20–C18–O19 and C6-C1-C18-O19 torsion angle of -149.10° and -149.31°. The larger torsion of the phenyl rings are due

Table 2: Optimized geometrical parameters of 3,5-DMBP obtained by B3LYP/6-31+G (d,p) density functional calculations.

Bond length*	Value(Å)	Exp(Å)	Bond angle*	Value(°)	Exp(°)
C1–C2	1.4048	1.401[c]	C1–C2–C3	120.99	120.8[c]
C2–C3	1.3927	1.378[b,c]	C2–C3–C4	118.33	120.9[c]
C3–C4	1.4048	1.389[b,c]	C3–C4–C5	122.04	118.2[c]
C4–C5	1.3961	1.384[b,c]	C4–C5–C6	118.41	121.7[c]
C5–C6	1.4023	1.382[b,c]	C2–C3–C8	121.29	120.6[c]
C2–H7	1.0852	0.953[a]	C4–C3–C8	120.37	121.2[c]
C3–C8	1.5108	1.507[c]	C1–C18–O19	119.67	119.4[c]
C4–H9	1.0883	–	C1–C18–C20	120.91	120.9[c]
C5–C10	1.5113	1.528[a]	O19–C18–C20	119.40	119.7[c]
C6–H11	1.0855	0.963[a]	C18–C20–C21	117.45	118.3[c]
C8–H12	1.0958	0.914[a]	C20–C21–C22	120.54	120.3[c]
C8–H13	1.0961	0.926[a]	C21–C22–C23	120.00	121.3[c]
C8–H14	1.0928	0.934[a]	C22–C23–C24	119.92	118.4[c]
C10–H15	1.0956	–	C23–C24–C25	120.13	121.1[c]
C1–C18	1.5009	1.493[c]			
C18–O19	1.2268	1.220[c]			
C18–C20	1.5022	1.492[c]			
C20–C21	1.4041	1.392[c]			
C21–C22	1.3913	1.379[c]			
C22–C23	1.3978	1.379[c]			
C23–C24	1.3954	1.379[c]			
C24–C25	1.3951	1.384[c]			
C21–H26	1.0847	1.013[a]			
C22–H27	1.0860	0.969[a]			
C23–H28	1.0862	0.963[a]			
C24–H29	1.0860	0.919[a]			
C25–H30	1.0844	0.924[a]			

* For numbering of atoms refer to Fig. 1.
[a] See Ref. [26].
[b] See Ref. [42].
[c] See Ref. [43].

to the large repulsive forces between the H atoms attached to the ortho-carbon atoms C6 and C25. The repulsion of H atoms at C6 and C25 is balanced by not only the π-conjugation of the carbonyl and aryl groups, but also by the intramolecular hydrogen bonding. The dihedral angle between the mean planes of the two benzene rings are is 43.21°. The difference in the C1–C18 = 1.500 Å and C20–C18 = 1.502 Å bond lengths indicates different degrees of conjugation in these C_{sp^2}-C_{aryl} bonds. The carbonyl O atom acts as a double hydrogen-bond receptor, involved in not only an intramolecular C–H···O hydrogen bond with one methyl H atom to form a six-membered ring, but also an intermolecular C–H···O hydrogen bond with other methyl H atoms of an adjacent molecule. The central bond angle C20–C18–C1 at the carbonyl group is 120.54°. The DFT/B3LYP values for all the bond lengths and bond an-

gles have deviation of 1% of the experimental results. The total energy obtained by the DFT structure optimization for the title compound was found to be -655.065869 Hartrees.

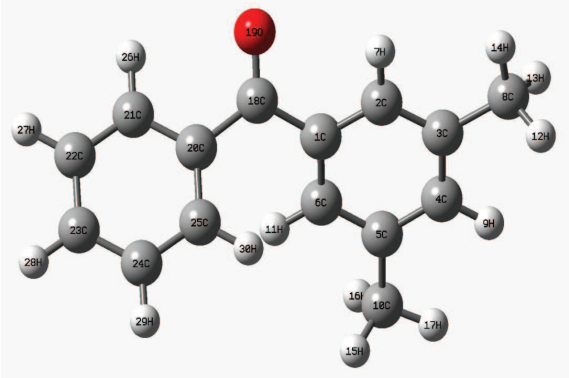

Figure 1: Molecular structure of 3,5-DMBP along with numbering of atom.

4.2 Vibrational analysis

The molecule has C_1 symmetry and 84 normal modes of vibrations, all active in infrared and Raman spectra. A detailed vibrational description can be given by means of normal coordinate analysis. The specific assignment to each frequency is attempted through Potential Energy Distribution (PED). For this purpose the full set of defined internal coordinates are given in Table 3. In order to obtain the normal modes in a molecular coordinate system, local symmetry coordinates for 2-chloro-4-fluorobenzophenone were defined as recommended by Fogarasi and Pulay [33] and were presented in Table 4. This method is also useful for determining the mixing of other modes. But mostly the maximum contribution is accepted to be the most significant mode. The observed FT-Raman and FT-IR bands with their relative intensities and calculated wavenumbers and assignments are given in Table 5. To understand the observed spectral features, comparison of the observed and simulated FTIR and FT-Raman spectra of 3,5-DMBP are presented in Figs. 2 and 3.

The RMS error of the observed and calculated frequencies (unscaled) of 3,5-DMBP was found to be 66.2 cm^{-1} respectively. This is quite obvious since the frequencies calculated on the basis of quantum mechanical force fields usually differ appreciably from observed frequencies. This is partly due to the neglect of anharmonicity and partly due to the approximate nature of the quantum mechanical methods. In order to reproduce the observed frequencies, the scale factors were refined and optimized via a least squares refinement algorithm which resulted into a weighed RMS deviation of 5.82 cm^{-1} between the experimental and scaled quantum mechanical (SQM) frequencies. The complete description of vibrational assignment is given below.

Table 3: Definition of internal coordinates of 3,5-DMBP.

No.(i)	Symbol	Type	Definition[a]
			Stretching
1–8	Ri	C–H	C2–H7, C4–H9, C6–H11, C21–H26, C22–H27, C23–H28, C24–H29, C25–H30
9–14	Ri	C–H (methyl)	C8–H12, C8–H13,C8–H14, C10–H15, C10–H16, C10–H17
15–16	Ri	C–C (methyl)	C3–C8, C5–C10
17–28	Ri	C–C	C1–C2, C2–C3, C3–C4, C4–C5, C5–C6, C6–C1, C21–C22, C22–C23, C23–C24, C24–C25, C25–C20, C20–C21
29–30	Ri	C–Cint	C1–C18, C18–C20.
31	Ri	C–O	C18–O19
			In-plane bending
32–47	γi	C–H	C1–C2–H7, C3–C2–H7, C3–C4–H9, C5–C4–H9, C5–C6–H11, C1–C6–H11, C20–C21–H26, C22–C21–H26, C21–C22–H27, C23–C22–H27, C22–C23–H28, C24–C23–H28, C23–C24–H29, C25–C24–H29, C24–C25–H30, C20–C25–H30
48–51	γi	C–C–C (methyl)	C2–C3–C8, C4–C3–C8, C4–C5–C10, C6–C5–C10
52–57	γi	C–C–H (methyl)	C5–C10–H15, C5–C10–H16, C5–C10–H17, C3–C8–H12, C3–C8–H13, C3–C8–H14
58–59	γi	C–O	C1–C18–O19, C20–C18–O19
60–63	γi	C–C	C2–C1–C18, C6–C1–C18, C21–C20–C18, C25–C20–C18
64	γi	C–C–C	C1–C18–C20
65–76	γi	Ring	C1–C2–C3, C3–C4–C5, C5–C6–C1, C2–C3–C4, C4–C5–C6, C6–C1–C2, C20–C21–C22, C21–C22–C23, C22–C23–C24, C23–C24–C25, C24–C25–C20, C25–C20–C21
77–82	αi	H–C–H	H12–C8–C13, H12–C8–C14, H13–C8–H14, H15–C10–H16, H15–C10–H17, H16–C10–H17
			Out-of-plane bending
83–90	ρi	C–H	H7–C2–C1–C3, H9–C4–C3–C5, H11–C6–C1–C5, H26–C21–C20–C22, H27–C22–C21–C23, H28–C23–C22–C24, H29–C24–C23–C25, H30–C25–C20–C24
91	ρi	C–O	O19–C18–C1–C20
92–93	ρi	C–C (methyl)	C10–C5–C4–C6, C8–C3–C2–C4
94–95	ρi	C–C	C18–C1–C2–C6, C18–C20–C21–C25
			Torsion
96–99	t i	CCCO	C6–C1–C12–O13, C2–C1–C12–O13, C19–C14–C12–O13, C15–C14–C12–O13
100–101	t i	C–CH3	C4(6)–C5–C10–(H15,H16,H17), C4(2)–C3–C8–(H12,H13,H14)
102–113	t i	Ring	C1–C2–C3–C4, C3–C4–C5–C6, C5–C6–C1–C2, C2–C3–C4–C5, C4–C5–C6–C1, C6–C1–C2–C3, C20–C21–C22–C23, C21–C22–C23–C24, C22–C23–C24–C25, C23–C24–C25–C20, C24–C25–C20–C21, C25–C20–C21–C22

[a] For numbering of atoms refer to Fig. 1.
Note: Only PED contributions greater than 10% are listed.

4.2.1 C–H vibrations

The C–H stretching vibrations in the benzene derivatives arises from non-degenerate mode 2 (3072 cm^{-1}) and two degenerate modes 7a and 7b (3047 cm^{-1}), 20a and 20b (3099 cm^{-1}). In this region, the bands are not appreciably affected by the nature of substituents [44]. Hence in the present investigation, the FT-IR bands at 3057, 3022 cm^{-1} and FT-Raman bands at 3059, 3009 cm^{-1} have been assigned to C–H stretching vibrations. In general most of them are weak in either the FT-Raman or FT-IR, with the exception of 3059 cm^{-1} which appears as very strong band in the FT-Raman spectra is assigned C–H in-phase stretching mode 2. The

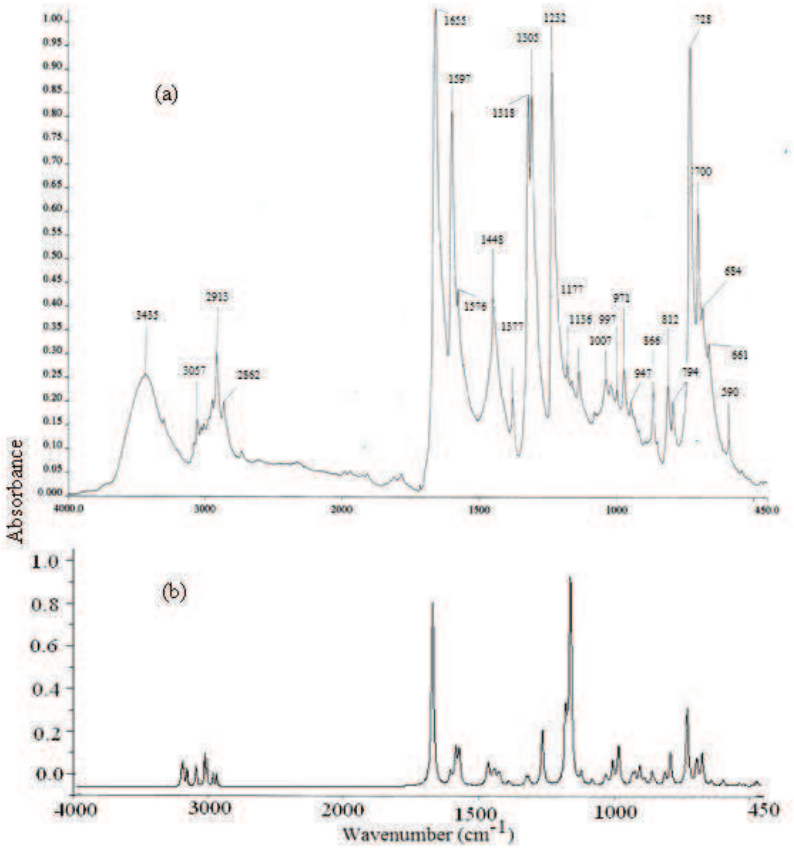

Figure 2: (a) Experimental FT-IR spectra of 3,5-DMBP (b) Simulated FT-IR spectra of 3,5-DMBP.

upper limit of frequency comparatively decreases may be due to the presence of methyl group.

The C–H in-plane bending vibrations appear in the region 1000–1520 cm^{-1} and C–H out-of-plane bending vibrations in the range of 700–1000 cm^{-1} [45]. The bands corresponding to the C–H in-plane bending modes 15 and 18b of benzene are observed at 1177 and 1081 cm^{-1} in the FT-IR spectra [15]. The corresponding calculated modes are dominated by C-H in-plane bending, and coupled mostly with CC stretching. The medium strong bands observed at 947, 898 and 866, 812 cm^{-1} in the FT-IR spectrum is assigned to 5, 17a and 10b modes of benzene. The mode corresponding to 10a is observed at 854 cm^{-1} in the FT-IR spectrum. All these calculated modes are in good agreement with the observed values.

4.2.2 C–C vibrations

The C–C stretching frequencies are generally predicted in the region 650–1650 cm^{-1} [45]. Several ring modes are affected by substitution in the aromatic ring; with heavy substituents, the bands tend to shift to somewhat lower wavenumbers and the greater the number of substituents on the ring, the broader the absorption regions [44]. In benzene, the C–C stretching

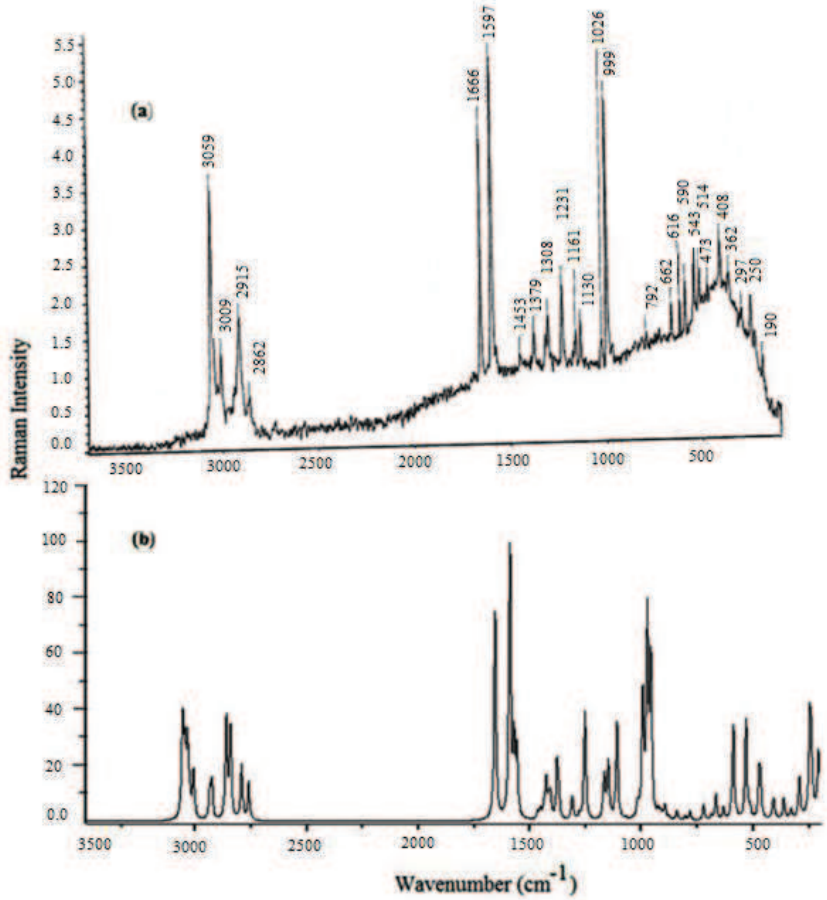

Figure 3: (a) Experimental FT-Raman spectra of 3,5-DMBP (b) Simulated FT-Raman spectra of 3,5-DMBP.

frequencies arise from the two doubly degenerated vibrations 8a and 8b (1596 cm^{-1}) and 19a and 19b (1485 cm^{-1}) and two non-degenerate modes 14 (1300 cm^{-1}) and 1 (998 cm^{-1}) which corresponds to skeletal vibrations [45]. The doubly degenerated 19a and 19b (1485 cm $^{-1}$) mode is basically a ring deformation since it involves both stretching and bending of the C–C bonds. The frequency of the vibrational pair 8 in substituted benzene is rather insensitive of substitution. The phenyl ring mode 8b manifests as very intense bands in both the FT-IR and FT-Raman spectra at 1597 cm^{-1} [15]. The modes corresponding to 8a are observed at 1576 cm^{-1} in the FT-IR spectrum. The strong bands observed at 1318, 1305 cm^{-1} in FT-IR spectrum are assigned to mode 14. From PED data most of calculated modes have more than 40% contribution of the CC-stretching mode.

The CC in-plane bending modes result from non-degenerate 12 (1010 cm^{-1}) and degen-

Table 4: Definition of local-symmetry coordinates and the values of corresponding scale factors used to correct the B3LYP/6-31G (d,p) (refined) force field of 3,5-DMBP.

No.(i)	Symbol[a]	Definition[b]	Scaling factors
1–8	ν(C-H)	R1,R2,R3,R4,R5,R6,R7,R8	0.920
9–10	CH_3ss	$(R9+R10+R11)/\sqrt{3}$, $(R12+R13+R14)/\sqrt{3}$	0.920
11–12	CH_3ips	$(2R9-R10-R11)/\sqrt{3}$, (2R12-R13-R14)$/\sqrt{3}$	0.940
13–14	CH_3ops	$(R10-R11)/\sqrt{2}$, $(R13-R14)/\sqrt{2}$	0.920
15–16	ν(C-Cme)	R15,R16	0.922
17–28	ν(C-C)	R17,R18,R19,R20,R21,R22,R23,R24,R25,R26,R27,R28	0.922
29–30	ν(C-Cint)	R29,R30	0.922
31	ν(C-O)	R31	0.922
32–39	β(C-H)	$(\gamma32-\gamma33)/\sqrt{2}$,$(\gamma34-\gamma35)/\sqrt{2}$, $(\gamma36-\gamma37)/\sqrt{2}$,$(\gamma38-\gamma39)/\sqrt{2}$, $(\gamma40-\gamma41)/\sqrt{2}$, $(\gamma42-\gamma43)/\sqrt{2}$, $(\gamma44-\gamma45)/\sqrt{2}$, $(\gamma46-\gamma47)/\sqrt{2}$	0.950
40–41	β(C-Cme)	$(\gamma48-\gamma49)/\sqrt{2}$,$(\gamma50-\gamma51)/\sqrt{2}$	0.950
42–43	CH_3sb	$(-\gamma52-\gamma53-\gamma54+\alpha77+\alpha78+\alpha79)/\sqrt{6}$, $(-\gamma55-\gamma56-\gamma57+\alpha80+\alpha81+\alpha82)/\sqrt{6}$	0.915
44–45	CH_3ipb	$(-\alpha77-\alpha78+2\alpha79)/\sqrt{6}$, $(-\alpha80-\alpha81+2\alpha82)/\sqrt{6}$	0.915
46–47	CH_3opb	$(\alpha77-\alpha78)/\sqrt{2}$, $(\alpha80-\alpha81)/\sqrt{2}$	0.915
48–49	CH_3ipr	$(2\gamma52-\gamma53-\gamma54)/\sqrt{6}$, $(2\gamma55-\gamma56-\gamma57)/\sqrt{6}$	0.915
50–51	CH_3opr	$(\gamma53-\gamma54)/\sqrt{2}$, $(\gamma56-\gamma57)/\sqrt{2}$	0.915
52	β (CO)	$(\gamma58-\gamma59)/\sqrt{2}$	0.950
53–54	β (CC)	$(\gamma60-\gamma61)/\sqrt{2}$, $(\gamma62-\gamma63)/\sqrt{2}$	0.950
55	β (CCC)	$\gamma64$	0.990
59–57	β Rtrig	$(\gamma65-\gamma66+\gamma67-\gamma68+\gamma69-\gamma70)/\sqrt{6}$, $(\gamma71-\gamma72+\gamma73-\gamma74+\gamma75-\gamma76)/\sqrt{6}$	0.990
58-59	β Rsym	$(-\gamma65-\gamma66+2\gamma67-\gamma68-\gamma69+2\gamma70)/\sqrt{12}$, $(-\gamma71-\gamma72+2\gamma73-\gamma74-\gamma75+2\gamma76)/\sqrt{12}$	0.990
60–61	β Rasym	$(\gamma65-\gamma66+\gamma68-\gamma69)/2$, $(\gamma71-\gamma72+\gamma74-\gamma75)/2$	0.990
62–69	ω(C-H)	$\rho83$,$\rho84$,$\rho85$,$\rho86$,$\rho87$,$\rho88$,$\rho89$,$\rho90$	0.976
70	ω(C-O)	$\rho91$	0.976
71–72	ω(C-Cme)	$\rho92$,$\rho93$	0.976
73–74	ω(C-C)	$\rho94$,$\rho95$	0.976
75–76	τ(CCCO)	$t96,97,t98,99$	0.935
77–78	$\tau(CH_3)$	$t100,t101$	0.831
79-80	τ Rtrig	$(t102-t103+t104-t105+t106-t107)/\sqrt{6}$, $(t108-t109+t110-t111+t112-t113)/\sqrt{6}$	0.935
81-82	τ Rasy	$(-t102+2t103-t104-t105+2t106-t107)/\sqrt{12}$, $(-t108+2t109+t110-t111+2t112-t113)/\sqrt{12}$	0.935
83-84	τ Rsym	$(t102-t104+t105-t107)/2$, $(t108-t110+t111-t113)/2$	0.935

Abbreviations: ν, stretching; β, in plane bending; ω, out of plane bending; τ, torsion, tri, trigonal deformation, sym, symmetric deformation, asy, asymmetric deformation, int, inter -ring.

[a] These symbols are used for description of the normal modes by PED in Table 5.

[b] The internal coordinates used here are defined in table given in Table 3.

erate 6a and 6b (606 cm^{-1}) modes of benzene. The strong band at 684 cm^{-1} and weak band at 513 cm^{-1} in the FT- IR are assigned to the 6a mode of benzene [15, 45]. The modes corresponding to 6b are observed as a medium strong band in the FT-IR spectrum at 590 and 473 cm^{-1}. Modes 6a and 6b mix with several other vibrations. In spite of this mixing, these vibrations retain their essential C–C–C bending character in the appropriate ratio for these modes. The medium strong band at 997 cm^{-1} in FT-IR and very strong band at 999 cm^{-1} in the FT-Raman can be identified as the breathing mode, an assignment which is also supported

Table 5: Detailed assignments of fundamental vibrations of 3,5-DMBP by normal mode analysis based on SQM force field calculations using B3LYP/6-31+G (d,p).

No	Experimental (cm^{-1})		Scaled frequencies (cm^{-1})	I_{IR}[b]	I_{RA}[c]	PED (%)[d]
	FT-IR	FT-Raman				
1	3057m	3059vs	3058	0.084	39.3	vCH (99)
2	-	-	3054	0.104	37.9	vCH (99)
3	-	-	3049	0.115	31.4	vCH (99)
4	-	-	3043	0.139	30.5	vCH (99)
5	-	-	3037	0.104	29.3	vCH (99)
6	-	-	3033	0.106	32.1	vCH (99)
7	3022w	-	3024	0.035	15.5	vCH (99)
8	-	3009m	3008	0.106	19.1	vCH (99)
9	3000w	-	3003	0.060	10.9	CH3ips (98)
10	-	-	2979	0.007	1.48	CH3ips (99)
11	2933w	-	2933	0.105	13.1	CH3ss (93)
12	2913m	2915m	2931	0.092	12.6	CH3ss (97)
13	2862m	2862w	2830	0.027	6.07	CH3ops (97)
14	-	-	2826	0.018	4.16	CH3ops (92)
15	1655vs	1656vs	1656	0.864	75.3	vCO (74)
16	1597vs	1597vs	1590	0.081	100.0	vCC (60), βCH(18)
17	-	-	1581	0.060	28.5	vCC (64), βCH (23)
18	1576s	-	1578	0.080	24.6	vCC (60), βCH(17), βR1sym(8)
19	-	-	1553	0.084	14.1	vCC (65), βCH(22), βR2asy (7)
20	-	-	1465	0.030	4.05	βCH(60), vCC (30)
21	-	-	1464	0.034	3.88	CH3ipb (29), CH3opb (21), CH3ips (11)
22	1448s	1453vw	1453	0.109	5.21	CH3ipb (67)
23	-	-	1443	0.053	4.57	CH3opb (47), CH3ipb (33)
24	-	-	1438	0.069	7.53	CH3opb (56), CH3ipb (20)
25	-	-	1425	0.067	15.1	βCH (58), vCC (35)
26	-	-	1407	0.050	9.71	vCC(41), CH3opb (15), βCH (14)
27	-	-	1395	0.013	4.00	vCC(34), CH3opb (21), βCCme (16), βCH (14)
28	1377m	1379w	1379	0.024	23.1	CH3sb(76)
29	-	-	1361	0.006	3.72	CH3sb (80), vCCme (11)
30	1318vs	-	1319	0.020	3.26	vCC (71), βCH (23)
31	1305vs	1305w	1316	0.031	5.20	vCC (67), βCH (33)
32	-	-	1295	0.017	1.94	βCH (43), vCC (36)
33	-	-	1274	0.019	3.77	vCCme (22), vCC(21), βR1tri (20), vCCint (13), βCH (13)
34	1232vs	1231m	1262	0.073	10.9	vCCint (39), βCH (17), vCC (15)
35	1177m	1161w	1188	0.040	2.02	βCH (45), vCC (29)
36	-	-	1152	0.890	19.7	βCH (75), vCC (21)
37	-	-	1148	1.000	21.0	βCH (47), vCCme (27), vCC (19)
38	1136m	1136w	1140	0.207	7.50	βCH (77), vCC (22)
39	1081w	-	1106	0.050	20.6	βCH (52), vCC (40)
40	-	-	1055	0.009	1.42	vCC (36), vCCint (31), βCH (15)
41	1037m	-	1033	0.016	2.50	CH3ipr (71)
42	1018m	1026w	1026	0.039	4.10	CH3opr (60), CH3ips (18)
43	-	-	1017	0.047	8.95	CH3ipr (66)
44	997m	999vs	1003	0.045	16.6	vCC (50), βCH (19), CH3opr (12)
45	-	-	993	0.107	43.1	CH3opr (34), βR2tri (24), vCC (18)
46	-	-	984	0.060	26.3	βR1tri (46), vCC(41)
47	971m	-	974	0.191	80.0	βR2tri (45), vCC (38)

Table 5: (Continued)

No	Experimental (cm^{-1})		Scaled frequencies (cm^{-1})	I_{IR} [b]	I_{RA} [c]	PED (%) [d]
	FT-IR	FT-Raman				
48	-	-	969	0.114	48.5	ωCH (84), TRtri2 (12)
49	-	-	955	0.021	44.9	vCC (28), ωCH (25), CH3opr (13), vCCme (10)
50	947w	-	954	0.019	37.6	ωCH (33), vCC (33), τR1tri (23)
51	918vw	-	924	0.063	5.64	vCCme (30), vCC(23), ωCH (10)
52	-	-	913	0.060	4.34	ωCH (84)
53	898vw	-	902	0.050	4.21	ωCH (80)
54	866m	-	887	0.035	2.49	ωCH (90)
55	854vw	-	859	0.024	1.09	ωCH (63), τR1tri (23)
56	812m	-	836	0.020	2.08	ωCH (99)
57	794m	792vw	795	0.041	1.34	vCC (19), βCO (15), vCCint (13), vCCme (12), βR1sym (11)
58	-	-	770	0.025	0.87	ωCH (35), ωCO (20), ωCC (16), τR2tri (14)
59	728vs	-	723	0.353	5.94	ωCH (37), τR1tri (33), ωCC (13)
60	700s	-	688	0.129	2.74	τR1tri (30), ωCH(28), τR2tri(14)
61	684s	-	662	0.081	5.31	βR2sym (31), τR2tri (17)
62	661m	662w	634	0.027	5.37	τR2tri (53), ωCH (12), τR1tri (10)
63	590w	590m	588	0.029	33.8	βR2asy (69), βR2sym (14)
64	549vw	543m	571	0.004	3.63	βCCC (21), τR2tri (11)
65	513vw	514m	532	0.015	37.0	βR1sym (30), vCCme (20),CH3ips (17), vCC (14)
66	-	473vw	504	0.002	2.97	βR1asy(45), vCCme (12), βR1sym (10)
67	463vw	-	464	0.017	13.2	τR1sym (49), ωCCme (30)
68	-	-	440	0.002	1.67	τR1asy (19), βCCme (16), ωCCme (15), ωCC(12)
69	-	408m	427	0.003	1.74	τR1asy(26), τR2sym (17), ωCCme (13)
70	-	-	400	0.004	3.74	τR2sym(40), βCCme (32)
71	-	362vw	368	0.052	4.64	τR2asy (28), βCCme (28)
72	-	-	357	0.051	4.48	βCO(36), τR2asy (12)
73	-	297vw	290	0.008	12.7	CH3ips (44), βCCme (36)
74	-	250w	237	0.001	29.0	βCCme (35), CH3ips (31), βCC (11), vCCint (10)
75	-	-	219	0.001	9.00	ωCCme (20), βCC (19), τR1sym (13)
76	-	190vw	196	0.001	16.7	τR1asy (25), βCC (19), ωCCme (18)
77	-	-	175	0.006	36.6	βCC (27), βCCme (14), τR1asy (12), ωCCme (10)
78	-	-	157	0.001	8.97	ωCCme (43), ωCH (11), τR2asy (10)
79	-	-	111	0.001	24.1	τCCCO (45), ωCO (22)
80	-	-	72	0.001	15.0	ωCC (35), βCCC (17)
81	-	-	49	0.001	3.45	τCCCO (53), βCCC (17), βCC (16)
82	-	-	32	0.008	13.2	τCH3 (62), ωCCme (14)
83	-	-	31	0.007	13.1	τCH3 (56), τCCCO (14),CH3ips (11), ωCCme (11)
84	-	-	25	0.004	12.8	τCCCO (74), τCH3 (13)

[a] Abbreviations: v, stretching; β, in plane bending; ω, out of plane bending; t, torsion, ss, symmetrical stretching, ips, in-plane stretching, ops, out of plane stretching , sb, symmetrical bending, ipb, in-plane bending, opb, out-of -plane bending;, int, inter ring, ipr, in-plane rocking, opr, out -of- plane rocking;tri, trigonal deformation, sym, symmetrical deformation, asy, asymmetric deformation, vs, very strong; s, strong; ms, medium strong; w, weak; vw, very weak.

[b] Relative absorption intensities normalized with highest peak absorption equal to 1.

[c] Relative Raman intensities calculated by Eq. (1) and normalized to 100.

[d] Only PED contributions β10% are listed.

by computations.

The CC out-of-plane bending vibrations are derived from the non-degenerate 4 (703 cm^{-1}) and degenerate 16a and 16b (404 cm^{-1}) modes of benzene. The medium strong band ob-

served at 700 cm^{-1} in the FT-IR is assigned to the non-degenerated benzene mode 4. The mode corresponding to 16b is observed at 408 cm^{-1} in the FT-Raman spectrum. These assignments are in agreement with values given in the literature [15].

4.2.3 C–CO–C group vibrations

The carbonyl stretching vibrations in ketones are expected in the region 1680–1715 cm^{-1}. In benzophenone [15], the sharp intense band in the Raman spectrum at 1650 cm^{-1} is assigned to the C=O stretching mode. In our case the very strong band at 1655 cm^{-1} in the FT-IR and also very strong band at 1656 cm^{-1} in the FT-Raman is assigned as the C=O stretching vibration. The reported value of 1655 cm^{-1} for the C=O stretching vibration in our title molecule is below the expected range and may be due to the conjugation of the C=O bond with the aromatic ring which may increase its single bond character, resulting in lowered values of carbonyl-stretching wavenumbers [46]. The in-plane and out-of-plane bending modes of the C=O bond are calculated at 357 cm^{-1} and 110 cm^{-1} comparable with those reported by Sett *et al.*, [21]. The very strong band observed at 1232 cm^{-1} in the FT-IR and 1231 cm^{-1} in the FT-Raman spectra are assigned to $\nu(CC_{int})$ mode of the ketone. This is compare closely to the calculated value of 1262 cm^{-1}. These assignments are in good agreement with data reported by Kolev *et al.* [15].

4.2.4 Methyl group vibrations

The asymmetric and symmetric stretching modes of methyl group attached the benzene ring are usually downshifted due to electronic effects [47] and are expected in the range 2850–3000 cm^{-1} for asymmetric and symmetric stretching vibrations [45]. The first of these results from the asymmetric stretching CH_3 mode in which two C–H bonds of the methyl group are extending while the third one is contracting. The second arises from symmetrical stretching CH_3 in which all three of the C–H bonds extend and contract in phase. The two CH_3ss frequencies are calculated to be 2933 and 2931 cm^{-1}. Which are well comparable with the experimental values observed at 2913(m) cm^{-1}, 2862(m) cm^{-1} in FT-IR and 2915 (m) cm^{-1}, 2862 (w) cm^{-1} in FT-Raman spectra. The frequency of calculated values of CH_3 ips frequencies are 3003 cm^{-1} (not observed experimentally) and 2979 cm^{-1} (observed only in FT-IR spectra at 2933 (vw) cm^{-1}). The two CH_3ops modes are calculated at 2830 and 2824 cm^{-1} both are not observed from experiment. In many molecules the symmetric deformation (labeled CH_3sb and CH_3 ipb in the Table 2) appears with an intensity varying from medium to strong and expected in the range 1380±25 cm^{-1} [45]. The two CH_3sb frequencies are calculated at 1379 and 1361 cm^{-1}. Out of these two modes one is observed in the FT-IR and FT-Raman spectra at 1377 and 1379 cm^{-1}. The CH_3ipb are calculated to be 1464 cm^{-1} (not observed experimentally) and 1453 cm^{-1} (1448 (s) cm^{-1} in FT-IR, 1453 (vw) cm^{-1} in Raman spectra). The asymmetric deformations are expected in the range 1400–1485 cm^{-1} [45]. The CH_3opb are calculated at 1443 cm^{-1} and 1438 cm^{-1}. Experimentally no bands are observed. Aromatic molecules display an in-plane methyl rocking (labeled CH_3ipr in the Table 5) in the neighbourhood of 1045 cm^{-1} [45]. The out-of-plane rocking in the region 970±70 cm^{-1} [45] is more difficult to find among the C–H out-of-plane deformations. The two CH_3ipr modes are

calculated to be 1033 cm^{-1} (observed in FT-IR spectrum at 1037 (m) cm^{-1}) and 1017 cm^{-1} (not observed in the experiment). The two CH_3opr modes are calculated at 1026 cm^{-1} (observed in the FT-IR at 1018 (m) cm^{-1} and the FT-Raman spectra at 1026 (w) cm^{-1}) and 993 cm^{-1} (not observed in the experiment). The two torsion frequencies have the calculated values 32 cm^{-1} and 31 cm^{-1}.

The calculated values of ν (C–CH_3) are 1274 and 924 cm^{-1}. The experimentally observed values in the FT-IR spectrum at 918 cm^{-1} confirms the assignment on a comparison with the calculated values. Regarding the in-plane bending frequency β (C–CH_3) the calculations indicate from PED only one value at 237 cm^{-1} which is comparable with the Raman line at 250 cm^{-1}. The frequency at 290 cm^{-1} which is expected in the region of β (C–CH_3), is appearing as 36%, while the first contribution 44% is for CH_3ips. The latter cannot be considered for CH_3ips just on the basis of PED percentage as the region of CH_3ips is about 2800–3000 cm^{-1}. The author preferred 290 cm^{-1} for β (C–CH_3) where as a contribution of 44% of CH_3ips mode can be retained as it is .The two C–CH_3 out of plane bending modes ω (C–CH_3) as per the PED is assigned to frequencies 219 and 72 cm^{-1}.These are not observed experimentally.

5 NBO analysis

The Natural bond orbital analysis provides an efficient method for studying intra- and intermolecular bonding and interaction among bonds, and also provides a convenient basis for investigating charge transfer or conjugative interaction in molecular systems. Some electron donor orbital, acceptor orbital and the interacting stabilization energy resulting from the second-order micro disturbance theory are reported [48,49]. The result of interaction is a loss of occupancy from the concentration of electron NBO of the idealized Lewis structure into an empty non-Lewis orbital. For each donor (i) and acceptor (j), the stabilization energy $E(2)$ associated with the delocalization $i \rightarrow j$ is estimated as

$$E(2) = -n_\sigma \frac{\langle \sigma|F|\sigma\rangle^2}{{\epsilon_\sigma}^2 - \epsilon_\sigma} = -n_\sigma \frac{{F_{ij}}^2}{\Delta E},$$

where $\langle \sigma|F|\sigma\rangle^2$ or ${F_{ij}}^2$ is the Fock matrix element i and j NBO orbitals, ${\epsilon_\sigma}^*$ and ϵ_σ are the energies of σ and σ^* NBOs and n_σ is the population of the donar σ orbital.

NBO analysis has been performed on the molecule at the DFT/B3LYP/6-31+G (d, p) level in order to elucidate the intramolecular, rehybridization and delocalization of electron density within the molecule, which are presented Table 6. The most important interaction (n–σ^*) energies, related to the resonance in the molecules, are electron donation from the LP(2)O atoms of the electron donating groups to the anti-bonding acceptor σ^* (C–C) of the phenyl ring (LP2O19$\rightarrow\sigma^*$ (C18–C20)) = 19.42 kJ/mol. This larger energy shows the hyperconjugation between the electron donating groups and the phenyl ring. The another intramolecular hyperconjugative interactions are formed by the orbital overlap between σ (C–C) $\rightarrow\sigma^*$ (C–C), π (C–C) $\rightarrow\pi^*$ (C–C) and bond orbitals, which results in ICT (Intra molecular charge transfer)

Table 6: Second order perturbation theory analysis of fock matrix in NBO basis for 3,5-DMBP.

Donor (i)	Type	ED/e	Acceptor (j)	Type	ED/e	$E(2)^a$ (kJ mol^{-1})	$E(j)-E(i)^b$ (a.u.)	$F(i,j)^c$ (a.u.)
C1–C2	σ	1.97174	C1–C6	σ^*	0.02072	3.43	1.26	0.059
			C1–C18	σ^*	0.06322	1.45	1.12	0.036
C1–C6	σ	1.97378	C1–C2	σ^*	0.02072	3.41	1.26	0.059
			C18–O19	σ^*	0.01037	1.66	1.28	0.041
	π	1.66035	C2–C3	π^*	0.30178	17.67	0.29	0.065
			C4–C5	π^*	0.32229	19.81	0.29	0.067
			C18–O19	π^*	0.16035	14.31	0.27	0.058
C1–C18	σ	1.97750	C1–C2	σ^*	0.02072	1.52	1.22	0.038
			C1–C6	σ^*	0.02145	1.84	1.22	0.042
			C5–C6	σ^*	0.02269	2.19	1.22	0.046
C2–C3	σ	1.97553	C1–C2	σ^*	0.02072	2.7	1.26	0.052
			C1–C18	σ^*	0.06322	2.77	1.13	0.05
	π	1.64958	C1–C6	π^*	0.36116	20.86	0.28	0.068
			C4–C5	π^*	0.32229	19.17	0.28	0.066
C3–C4	σ	1.97548	C2–C3	σ^*	0.02083	2.81	1.28	0.054
			C4–C5	σ^*	0.02115	2.76	1.27	0.053
			C5–C10	σ^*	0.01443	3.37	1.1	0.054
C3–C8	σ	1.98491	C1–C2	σ^*	0.0207	2.39	1.19	0.048
			C2–C3	σ^*	0.02083	1.8	1.21	0.042
			C4–C5	σ^*	0.02115	2.38	1.2	0.048
C4–C5	σ	1.97594	C3–C4	σ^*	0.02251	2.82	1.26	0.053
			C3–C8	σ^*	0.01449	3.1	1.11	0.052
	π	1.65726	C1–C6	π^*	0.36116	19.56	0.28	0.066
			C2–C3	π^*	0.30178	19.73	0.29	0.068
C5–C6	σ	1.97477	C1–C6	σ^*	0.02145	2.81	1.26	0.053
			C1–C18	σ^*	0.06322	3.25	1.13	0.054
			C4–C5	σ^*	0.02115	2.85	1.27	0.054
C5–C10	σ	1.98509	C1–C6	σ^*	0.02145	2.4	1.19	0.048
			C3–C4	σ^*	0.02251	2.37	1.19	0.047
C8–H12	σ	1.98148	C2–C3	σ^*	0.02083	2.13	1.09	0.043
			C2–C3	π^*	0.30178	2.88	0.54	0.038
C8–H13	σ	1.98002	C2–C3	σ^*	0.02083	1.86	1.09	0.04
			C2–C3	π^*	0.30178	3.27	0.54	0.04
C8–H14	σ	1.99043	C3–C4	σ^*	0.02251	4.28	1.07	0.061
C10–H15	σ	1.98189	C4–C5	σ^*	0.02115	2.22	1.08	0.044
			C4–C5	π^*	0.32229	2.84	0.54	0.038
C10–H16	σ	1.98031	C4–C5	σ^*	0.02115	1.79	1.08	0.039
			C4–C5	π^*	0.32229	3.31	0.54	0.041
C10–H17	σ	1.99045	C5–C6	σ^*	0.02269	4.26	1.07	0.061
C18–O19	σ	1.99388	C1–C6	σ^*	0.02145	1.25	1.63	0.04
			C1–C18	σ^*	0.06322	0.84	1.49	0.032
	π	1.96950	C1–C6	π^*	0.36116	3.72	0.4	0.038
			C20–C25	π^*	0.36322	3.66	0.39	0.037
C20–C25	σ	1.97520	C18–O19	σ^*	0.01037	1.62	1.28	0.041
			C18–C20	σ^*	0.06417	1.35	1.13	0.035
	π	1.63925	C18–O19	π^*	0.16035	13.93	0.27	0.058
			C21–C22	π^*	0.29426	19.59	0.28	0.068
			C23–C24	π^*	0.32441	19.10	0.28	0.065
C21–C22	σ	1.98069	C18–C20	σ^*	0.06417	2.95	1.13	0.052
			C20–C21	σ^*	0.02149	2.46	1.26	0.05
	π	1.65189	C20–C25	π^*	0.36322	19.1	0.28	
			C23–C24	π^*	0.32441	21.4	0.28	0.069
C23–C24	σ	1.98138	C22–C23	σ^*	0.01591	2.08	1.26	0.046
			C22–H27	σ^*	0.01224	2.34	1.17	0.047
	π	1.65365	C20–C25	π^*	0.36322	21.27	0.28	0.069
			C21–C22	π^*	0.29426	17.96	0.28	0.065

Table 6: (Continued).

Donor (i)	Type	ED/e	Acceptor (j)	Type	ED/e	$E(2)^a$ (kJ mol^{-1})	$E(j)-E(i)^b$ (a.u.)	$F(i,j)^c$ (a.u.)
O19	LP1	1.97812	C1–C18	σ^*	0.06322	1.78	1.12	0.04
			C18–C20	σ^*	0.06417	1.74	1.12	0.04
	LP2	1.89100	C1–C18	σ^*	0.06322	19.22	0.69	0.104
			C18–C20	σ^*	0.06417	19.42	0.69	0.104
C2–C3	π^*	1.64958	C8–H12	σ^*	0.00776	0.8	0.4	0.04
			C8–H13	σ^*	0.00811	0.9	0.4	0.043
C4–C5	π^*	1.65726	C10–H15	σ^*	0.00763	0.84	0.4	0.04
			C10–H16	σ^*	0.00828	1	0.4	0.044
C18–O19	π^*	0.16035	C1–C6	π^*	0.36116	82.41	0.02	0.063
			C20–C25	π^*	0.36322	123.4	0.01	0.062

[a] $E(2)$ means energy of hyper conjugative interaction (stabilization energy).
[b] Energy difference between donor and acceptor i and j NBO orbitals.
[c] $F(i,j)$ is the Fock matrix element between i and j NBO orbitals.

causing stabilization of the system. These interactions are observed as increase in electron density (ED) in C–C antibonding orbital that weakens the respective bonds. The electron density of conjugated bond of benzene ring (∼1.97e) clearly demonstrate strong delocalization. The π^* (C18–O19) of the NBO conjugated with π^* (C1–C6) and π^* (C20–C25) resulting to an enormous stabilization of 82.14 and 123.40 kJ/mol respectively.

6 Mulliken atomic charges

The charge distribution of 3,5-DMBP shows that the carbon atom attached with hydrogen atoms is negative, whereas the remaining carbon atoms are positively charged. The oxygen atoms have more negative charges whereas all the hydrogen atoms have positive charges. The maximum atomic charge is obtained for C1 and C20 when compared with other atoms.

Table 7: Atomic charges for optimized geometry of 3,5-DMBP at B3LYP/6-31+G (d) level.

Atom No.	Atomic charge (e)	Atom No.	Atomic charge (e)
C1	1.000	H16	0.167
C2	0.138	H17	0.149
C3	0.278	C18	-0.750
C4	-0.645	O19	-0.374
C5	0.533	C20	0.845
C6	-0.948	C21	-0.090
H7	0.144	C22	0.100
C8	-0.610	C23	-0.128
H9	0.119	C24	-0.161
C10	-0.509	C25	-0.708
H11	0.132	H26	0.151
H12	0.162	H27	0.131
H13	0.165	H28	0.129
H14	0.155	H29	0.128
H15	0.162	H30	0.136

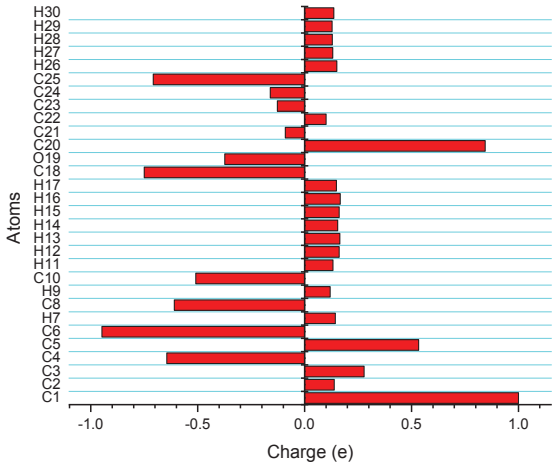

Figure 4: Atomic charge distribution of 3,5-DMBP.

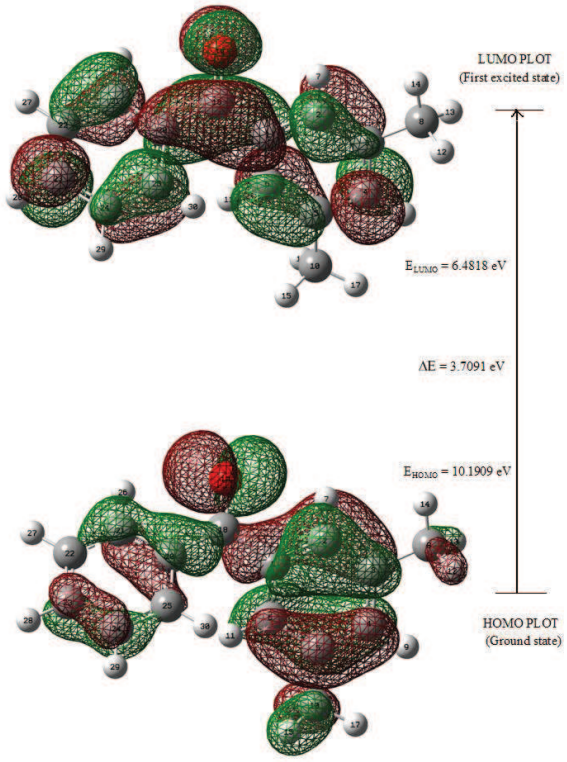

Figure 5: The atomic orbital components of the frontier molecular orbital of 3,5-DMBP.

This is due to the attachment of negatively charged carbon (C18) atom. Illustration of atomic charges plotted is shown in Fig. 4. Negatively charged lone pair oxygen (O19) atom shows that charge is transferred from O to H (O19→H7 and O19→H26). The calculated Mulliken charges of H7 (0.144e), H26 (0.151e) and O19 (-0.374e) taking part in intramolecular charge transfer is revealed in the Natural Bond Orbital analysis. Carbon atoms (C8 and C10) are more negatively charged which indicates the charge transfer from H to C (see Table 7).

7 HOMO, LUMO energy gap

Both the highest occupied molecular orbital (HOMO) and lowest unoccupied molecular orbital (LUMO) are the main orbital take part in chemical stability [50]. The HOMO represents the ability to donate an electron, LUMO as an electron acceptor represents the ability to obtain an electron. The HOMO and LUMO energy calculated by B3LYP/6-31 + G(d, p) method as shown below

HOMO energy (B3LYP) = 10.1909 eV
LUMO energy (B3LYP) = 6.4818 eV
HOMO-LUMO energy gap (B3LYP) = 3.7091 eV

The HOMO is located over the phenyl ring and the methyl groups attached to the phenyl ring. The HOMO→LUMO transition implies an electron density transfer to the methyl group from

Table 8: Thermodynamic properties for the 3,5-DMBP obtained by B3LYP/6-31+G (d, p) density functional calculations.

T(K)	S^0_m(J/mol K)	$C^0_{p,m}$ (J/mol K)	H^0_m (kJ/mol)	T(K)	S^0_m(J/mol K)	$C^0_{p,m}$ (J/mol K)	H^0_m (kJ/mol)
10	200.67	38.43	0.34	190	440.20	167.02	19.77
20	232.11	53.29	0.81	200	448.95	174.07	21.47
30	255.69	62.99	1.39	210	457.61	181.22	23.25
40	274.82	70.17	2.06	220	466.21	188.49	25.10
50	291.19	76.72	2.79	230	474.75	195.85	27.02
60	305.74	83.18	3.59	240	483.24	203.29	29.02
70	319.05	89.58	4.46	250	491.69	210.81	31.09
80	331.42	95.91	5.38	260	500.11	218.37	33.23
90	343.08	102.18	6.37	270	508.49	225.97	35.45
100	354.17	108.42	7.43	280	516.85	233.59	37.75
110	364.80	114.66	8.54	290	525.18	241.22	40.12
120	375.04	120.91	9.72	298.15	531.95	247.42	42.12
130	384.97	127.22	10.96	300	533.49	248.83	42.58
140	394.63	133.59	12.26	310	541.77	256.42	45.10
150	404.07	140.06	13.63	320	550.03	263.97	47.70
160	413.32	146.62	15.07	330	558.27	271.46	50.38
170	422.41	153.30	16.57	340	566.48	278.89	53.13
180	431.36	160.10	18.13	350	574.67	286.24	55.96

the phenyl ring. Moreover, these orbital significantly overlap in their position for 3,5-DMBP (Fig. 5). The calculated self-consistent field (SCF) energy of 3,5-DMBP is -655.065869 a.u. The HOMO and LUMO energy gap explains the eventual charge transfer interactions taking place within the molecule.

8 Thermodynamic properties

On the basis of vibrational analyses and statistical thermodynamics, the standard thermodynamic functions: heat capacity ($C^0_{p,m}$), entropy (S^0_m) and enthalpy (H^m_0) were calculated using perl script THERMO.PL [51] and are listed in Table 8. As observed from Table 8, the values of $C^0_{p,m}$, S^0_m and H^0_m all increase with the increase of temperature from 10 to 350 K , which is attributed to the enhancement of the molecular vibration as the temperature increases.

9 Conclusions

The FT-IR and FT-Raman measurements have been made for the 3,5-dimethylbenzophenone. The complete vibrational analysis and first order hyperpolarizability, NBO analysis, HOMO and LUMO analysis, thermodynamic properties of the title compound was performed on the basis of DFT calculations at the B3LYP/ 6-31+G (d, p) basis set. The consistency between the calculated and experimental FT-IR and FT-Raman data indicates that the B3LYP/ 6-31+G (d, p) method can generate reliable geometry and related properties of the title compound. The difference between the observed and scaled wave number values of most of the fundamentals is very small. Thermodynamic properties in the range from 100 to 500 K are obtained. The gradients of $C^0_{p,m}$ and S^0_m to the temperature decrease, but that of H^0_m increases, as the temperature increases.

Acknowledgments. One of the authors, K. Chaitanya, feels indebted to Prof. V. Krishna Kumar and Dr. Muthunatesan for valuable suggestions during the course of investigation and also to SAIF, Chennai; CECRI, Karikudi for recording the spectra. The author is highly grateful to Prof. T. Sundius for Molvib program. The author is thankful to Prof. V. Veeraiah for his keen interest and his valuable suggestions. K. Chaitanya is grateful to Prof. C. Santhamma for suggesting the problem and her constant supervision.

References

[1] M. Mahendra, B. Doreswamy, M. Sridhar, *et al.*, Struct. Chem. 15 (2004) 211.
[2] Y.B. Basavaraju and Devaraju, Indian J. Heterocyl. Chem. 11 (2002) 229.
[3] J. Wiesner, K. Fucik, K. Kettler, *et al.*, Bioorg. Med. Chem. Lett. 13 (2003) 1539.
[4] H. Koshima, W. Matsusaka, and H. Yu, J. Photochem. Photobiol. A Chem. 156 (2003) 83.
[5] A. Wrzyszczynshi, J. Bartoszewicz, G. L. Hug, *et al.*, J. Photochem. Photobiol. A Chem. 155 (2003) 253.

[6] P. N. Prasad and D. J. Williams, Introduction to Nonlinear Optical Effects in Molecules and Polymers (Wiley, NewYork, 1991).
[7] D. S. Chemla and J. Zyss, Nonlinear Optical Properties of Organic Molecules and Crystals (Academic Press, New York, 1987).
[8] S. Giorgianni, A. Passerini, A. Gambi, *et al.*, Spectrosc. Lett. 13 (1980) 445.
[9] J. Blazevic and L. Colombo, J. Raman Spectrosc. 11 (1981) 143.
[10] M. S. Mathur, J. Bradley Nelson, and G. C. Tabisz, Spectrosc. Lett. 14 (1981) 339.
[11] Ts. Kolev, B. Nikolova, B. Jordanov, and I. Juchnovski, J. Mol. Struct. 129 (1985) 1.
[12] S. Mohan, A. R. Prabakaran, K. Mahadevan, and M. S. Chandrasekaran, Indian J. Phys. B. 63 (1989) 340.
[13] I. Juchnovski, Ts. Kolev, and B. Stamboliyska, Spectrosc. Lett. 26 (1993) 67.
[14] D. Kirin and V. Volovsek, J. Chem. Phys. 106 (1997) 9505.
[15] Ts. M. Kolev and B. A. Stamboliyska, Spectrochim. Acta A 56 (1999) 119.
[16] N. A. Davydova, L. M. Babkov, J. Baran, *et al.*, J. Mol. Struct. 614 (2002) 167.
[17] V. Krishnakumar, S. Muthunatesan, G. Keresztury, and T. Sundius, Spectrochim. Acta A 62 (2005) 1081.
[18] W. Sasiadek, M. Maczka, E. Kucharska, *et al.*, J. Raman Spectrosc. 36 (2005) 912.
[19] T. V. Bezrodnaya, V. I. Melnik, G. A. Puchkovskaya, and L. I. Savranskii, J. Struct. Chem. 47 (2006) 194.
[20] L. Babkov, J. Baran, N. A. Davydova, *et al.*, J. Mol. Struct. 792 (2006) 73.
[21] P. Sett, T. Misra, S. Chattopadhyay, *et al.*, Vib. Spectrosc. 44 (2007) 331
[22] V. Volovsek, G. Baranovic, L. Colombo, and J. R. Durig, J. Raman Spectrosc. 22 (1991) 35.
[23] V. Volovsek, G. Baranovic, and L. Colombo, J. Mol. Struct. 266 (1992) 217.
[24] M. A. V. Ribeiro da Silva, L. M. P. F. Amaral, F. C. R. Guedes, and J. R. B. Gomes, J. Phys. Org. Chem. 19 (2006) 689.
[25] J. R. B. Gomes, L. M. P. F. Amaral, and M. A. V. Ribeiro da Silva, J. Phys. Org. Chem. 21 (2008) 365.
[26] W. Sasiadek, E. Kucharska, J. Hanuza, *et al.*, Vib. Spectrosc. 43 (2007) 165.
[27] J. Z. Wang, B. R. Nayak, D. Creed, *et al.*, Polymer 46 (2005) 6897.
[28] A. D. Becke, Phys. Rev. A 38 (1988) 3098.
[29] C. Lee, W. Yang, and R. G. Parr, Phys. Rev. B 37 (1988) 785.
[30] M. J. Frisch, G. W. Trucks, H. B. Schlegel, *et al.*, Gaussian 03, Revision E.01 (Gaussian, Inc., Wallingford CT, 2004).
[31] A. Frisch, A. B. Nielsen, A. J. Holder, *et al.*, Gaussview Users Manual (Gaussian, Inc., Pittsburg, 2000).
[32] G. Fogarasi, P. Pulay, in: Vibrational Spectra and Structure, Vol. 14, ed. J. R. Durig (Elsevier, Amsterdam, 1985) p.125; J. Baker, A. A. Jarzecki, and P. Pulay, J. Phys. Chem. A 102 (1998) 1412.
[33] P. Pulay, G. Fogarasi, F. Pang, and J. E. Boggs, J. Am. Chem. Soc. 101 (1979) 2550.
[34] T. Sundius, J. Mol. Struct. 218 (1990) 321.
[35] T. Sundius, Vibr. Spectrosc. 29 (2002) 89.
[36] E. D. Glendering, A. E. Reed, J. E. Carpenter, and F. Weinhold, NBO Version 3.1 (TCI, University of Wisconsin, Madison, 1998).
[37] P. L. Polavarapu, J. Phys. Chem. 94 (1990) 8106.
[38] G. Keresztury, S. Holly, J. Varga, G. Besenyei, A.Y. Wang, and J. R. Durig, Spectrochim. Acta A 49 (1993) 2007.
[39] E. B. Wilson, Jr., J. C. Decius, and P. C. Cross, Molecular Vibrations (McGraw-Hill, New York,

1955).
[40] W. J. Orville-Thomas, J. Chem. Phys. 19 (1951) 1162.
[41] Y. Morino and K. Kuchitsu, J. Chem. Phys. 20 (1952) 1809.
[42] A. A. Chumakov, I. I. Silvestrova, and K. Aleksandrov, Kristalografiya 2 (1957) 707.
[43] B. Kojic-Prodic, N. Bresciani-Pahor, and D. Horvatic, Acta Cryst. C 46 (1990) 430.
[44] N. P. G. Roeges, A Guide to Complete Interpretation of Infrared Spectra of Organic Structures (Wiley, New York, 1994).
[45] L. J. Bellamy, The Infra-red Spectra of Complex Molecules (Chapman and Hall Ltd., London, 1975); G. Varsanyi, Assignments for Vibrational Spectra of Seven Hundred Benzene Derivatives, Vols. 1 and 2 (Adam Hilger, London, 1974); G. Socrates, Infrared Characteristic Group Frequencies (John Wiley & Sons, England, 1980).
[46] D. Sajan, I. H. Joe, and V. S. Jayakumar, J. Raman Spectrosc. 37 (2006) 508.
[47] B. Smith, Infrared Spectral Interpretation-A Systematic Approach (CRC Press, New York, 1999).
[48] C. James, A. AmalRaj, R. Reghunathan, *et al.*, J. Raman Spectrosc. 37 (2006) 1381.
[49] L. J. Na, C. Z. Rang, and Y. S. Fang, J. Zhejiang Univ. Sci. B 6 (2005) 584.
[50] S. Gunasekaran, R. A. Balaji, S. Kumaresan, *et al.*, Can. J. Anal. Sci. Spectrosc. 53 (2008) 149.
[51] K. K. Irikura, THERMO. PL (National Institute of Standards and Technology, Gaithersburg, MD, 2002).